International Journal of
Nanoscience and Nanotechnology

Research Article 2025, Volume 21, Issue 1

Enhancing Effective Dielectric constant of As_2Se_3: Investigating the Impact of Metal and Titanium Dioxide Nanoparticle Size

Hossein Shahmirzaee[1], Abdolrasoul Gharaati[2], Abdoreza Kamaldar[2,3*]

Received 7/8/2024
Accepted 1/20/2025

DOI: 10.22034/ijnn.2025.2034868.2541

International Journal of Nanoscience and Nanotechnology

Abstract

The objective of this study is to propose a methodology for examining how the size of metal nanoparticles, specifically gold, silver, copper, and titanium dioxide, affects the dielectric constant of chalcogenide glasses. To achieve this, spherical nanoparticles with a volume fraction below 0.1, which minimize their interaction, are dispersed within the glasses. By employing the T-matrix method, the effective dielectric constant (EDC) of the composite medium is determined as a function of nanoparticle size (radius) and volume fraction at 635 nm wavelength. The corresponding diagrams are plotted to illustrate the outcomes. Finally, the findings reveal a substantial increase in the EDC of the composite medium as the radius of the nanoparticles grows, particularly when the volume fraction of the nanoparticles is increased. For instance, in the case of a 635nm wavelength and a volume fraction of 0.08, the magnitude of EDC exhibits a pronounced dependence on both the radius and type of nanoparticles. Specifically, when the nanoparticle radius is 10nm, the minimal EDC is observed with silver nanoparticles, whereas the maximal EDC is manifested with gold nanoparticles. Conversely, at a radius of 50nm, the minimal EDC is realized with gold nanoparticles, while the maximal EDC is attained with silver nanoparticles. Lastly, at a 100nm radius, the minimal EDC is associated with silver nanoparticles, and the maximal EDC is elicited by titanium dioxide nanoparticles.

Keywords: Effective Dielectric Constant, Nanoparticles, T-Matrix Method, Volume Fraction, Chalcogenide Glass

How to cite this article

Shahmirzaee H, Gharaati A, Kamaldar A. Enhancing Effective Dielectric constant of As_2Se_3: Investigating the Impact of Metal and Titanium Dioxide Nanoparticle Size. Int. J. Nanosci. Nanotechnol., 2025;1: 1-9. DOI: 10.22034/ijnn.2025.2034868.2541

1. Introduction

Chalcogenide glass (CG) is made from chalcogen elements, specifically sulfur, selenium, and tellurium. To create this glass, other elements like germanium, arsenic, antimony, and gallium are mixed. These glasses have a low phonon energy and cover a wide range from visible to infrared light [1].

Experiments have shown that chalcogenide glass can combine with impurities, leading to improved optical properties when metallic nanoparticles are distributed within it [2]. Rare elements like erbium, neodymium, and praseodymium can also be added to chalcogenide glass. These glasses find numerous applications in optical components. They can be utilized to produce ultra-fast optical switches, sensors, trackers, and distance sensors. Additionally, they have various applications in optical industries, communications, electronics, optoelectronics, mechatronics, and the military [3]. Maxwell-Grant theory, also known as the Maxwell-Grant approximation [4], is a widely recognized method used to study the linear optical behavior of compound mediums. This approximation is particularly suitable when one element acts as the host and the other as the guest. Several techniques are available to derive the theoretical equations of Maxwell-Grant, one of which is the local field method.

Recently [5] and other researchers [6,7] examined a compound medium consisting of metallic nanoparticles dispersed randomly in a glass matrix. In this system, the linear and nonlinear dielectric constants of the metallic nanoparticles, represented by ε_1 and ε_2 respectively, were considered. The compound medium was subjected to an applied electric field $(\vec{E}_0)$ directed along the z-axis. The electric field within the nanoparticles was denoted as E, assuming the nanoparticles had a spherical shape. By solving Maxwell's equations and applying appropriate boundary conditions, the electric field within the spherical nanoparticles was determined. The T-Matrix method [8-11] was one of the notable approaches used, assuming the quasi-static approximation was valid. This approximation implies that the dimensions of the linear

[1] *Malek Ashtar University of Technology, Shiraz, Iran.*

[2] *Department of Physics, Faculty of Science, Payame Noor University, P. O. Box 19395-3697, Tehran, Iran.*

[3] *Department of Education, District 1, Shiraz, Iran.*

E-mail: akamaldar@student.pnu.ac.ir

inhomogeneities, such as the radius of the nanoparticles, are much smaller than the wavelengths of radiation. For simplicity, the dielectric constant was considered scalar.

Additionally, the local field and plasma frequency were also explored in the analysis.[12] The compound medium in question consists of a glass matrix serving as the host and metallic nanoparticles acting as the guest. By applying an electric field to the compound medium and solving Maxwell's equations, the field distribution within the compound medium can be determined. This research aims to investigate the effect of the size of metal nanoparticles and titanium dioxide on increasing the optical properties of chalcogenide glass using the T-matrix method.

2. Modeling

The aim of this research is to propose a model that enhances the optical properties of glass oxides by incorporating metallic nanoparticles. The T-Matrix method is adapted for a compound system comprising metallic nanoparticles (guest) dispersed within silica glass (host). In this model, the dielectric constants of the host and guest, denoted as $\varepsilon(\omega)$ and $\varepsilon'(\omega)$, respectively, are taken into account [5].

$$\varepsilon(\omega)=\varepsilon_1(\omega)+\varepsilon_2\left|E_0\right|^2,$$
$$\varepsilon'(\omega)=\varepsilon_1'(\omega)+\varepsilon_2'\left|E\right|^2, \quad (1)$$

where ε_1 and ε_2 are the linear and nonlinear parts of the dielectric constant of the host medium (chalcogenide glass), respectively, and $\varepsilon_1', \varepsilon_2'$ are the linear and nonlinear parts of the dielectric constant of the guest medium. Moreover, $\vec{E}_0$ and $\vec{E}$ are respectively the applied electric field on the host medium and the electric field in the guest nanoparticles.

Examining the T-matrix method [5,7,8] and relevant prior research [12,13], this study explores the influence of nanoparticle size on the nonlinear optical properties of the compound medium. The expression for the electric field within the nanoparticles is provided as follows:

$$\vec{E}=\frac{3\varepsilon_e}{2\varepsilon_e+\bar{\varepsilon}_m}\vec{E}_0 \quad (2)$$

where $\bar{\varepsilon}_m$ is the renormalized dielectric constant of the metal [10], which is defined as

$$\bar{\varepsilon}_m=\varepsilon_m\frac{2F(k_m a)}{1-F(k_m a)},\quad F(x)=\frac{1}{x^2}-\frac{\cot x}{x}, \quad (3)$$

where ε_m is the metal dielectric constant, $k_m=k\sqrt{\varepsilon_m\mu_m}$, $k=\omega/c$ is the wave vector in a free space, μ_m is the magnetic permeability of metallic nanoparticles, a is the radius of nanoparticles, and ε_e is the EDC of the compound medium given by:

$$\varepsilon_e=\varepsilon_d\frac{(1+2f)\bar{\varepsilon}_m+2(1-f)\varepsilon_d}{(1-f)\bar{\varepsilon}_m+(f+2)\varepsilon_d}, \quad (4)$$

where f is the nanoparticles volume fraction, and ε_d is the dielectric constant of the host medium (glass) given by:

$$\varepsilon_d=\varepsilon_{1d}+\varepsilon_{2d}\left|E\right|^2, \quad (5)$$

where ε_{1d}, ε_{2d} are the linear and nonlinear parts of the dielectric constant of glass, respectively.

In this research, since the dielectric constant of metallic nanoparticles is assumed to be nonlinear, $\bar{\varepsilon}_m$ in Eq. (3) is corrected as

$$\bar{\varepsilon}_m=\varepsilon_{1m}Y+\varepsilon_{2m}\left|\vec{E}\right|^2,$$
$$Y=\frac{2\left[\frac{1}{(k_m a)^2}-\frac{\cot(k_m a)}{k_m a}\right]}{1-\left[\frac{1}{(k_m a)^2}-\frac{\cot(k_m a)}{k_m a}\right]}, \quad (6)$$

where $\varepsilon_{1m}, \varepsilon_{2m}$ are the linear and nonlinear parts of the dielectric constant of metal nanoparticles, respectively.

As shown in Appendix A, the electric field vector and the electric displacement can be obtained as

$$\vec{E}=x\vec{E}_0+x(\alpha-\beta x)\left|x\right|^2\left|\vec{E}_0\right|^2\vec{E}_0$$
$$+[x(\alpha-\beta x)(\alpha^*-\beta^* x^*+\alpha-\beta x)$$
$$-x^2\gamma]\left|x\right|^4\left|\vec{E}_0\right|^4\vec{E}_0, \quad (7)$$

Were

$$x=\frac{3\varepsilon_{1d}(1+2f)\varepsilon_{1m}Y+6\varepsilon_{1d}^2(1-f)}{\varepsilon_{1d}(5f+4)\varepsilon_{1m}Y+(1-f)(4\varepsilon_{1d}^2+\varepsilon_{1m}^2Y^2)} \quad (8)$$

$$\alpha=\frac{3\varepsilon_{1d}(1+2f)\varepsilon_{2m}(Y+1)}{3\varepsilon_{1d}(1+2f)\varepsilon_{1m}Y+6\varepsilon_{1d}^2(1-f)},$$
$$\beta=\frac{\varepsilon_{1d}(5f+4)\varepsilon_{2m}(Y+1)+(1-f)(2\varepsilon_{1m}Y\varepsilon_{2m})(Y+1)}{3\varepsilon_{1d}(1+2f)\varepsilon_{1m}Y+6\varepsilon_{1d}^2(1-f)}, \quad (9)$$
$$\gamma=\frac{(1-f)\varepsilon_{2m}^2(Y+1)^2}{3\varepsilon_{1d}(1+2f)\varepsilon_{1m}Y+6\varepsilon_{1d}^2(1-f)}.$$

and the electric displacement vector is obtained by $\vec{D}=\bar{\varepsilon}_m\vec{E}$. Using T-matrix method [5], the average of electric field and electric displacement can be written as

$$\langle\vec{E}\rangle=\left(1+\langle GT^{(1)}\rangle\right)\vec{E}_0+4\pi\langle GT^{(3)}\rangle\left|\vec{E}_0\right|^2\vec{E}_0$$
$$+4\pi\langle GT^{(5)}\rangle\left|\vec{E}_0\right|^4\vec{E}_0, \quad (10)$$

and,

$$\langle\vec{D}\rangle=[\varepsilon_{1d}(1+\langle GT^{(1)}\rangle)+\langle T^{(1)}\rangle]\vec{E}_0$$
$$+4\pi(\varepsilon_{1d}\langle GT^{(3)}\rangle+\langle T^{(3)}\rangle)\left|\vec{E}_0\right|^2\vec{E}_0 \quad (11)$$
$$+4\pi(\varepsilon_{1d}\langle GT^{(5)}\rangle+\langle T^{(5)}\rangle)\left|\vec{E}_0\right|^4\vec{E}_0,$$

where G is the Green's function, and $T^{(i)}$'s are T-matrices. As shown in Appendix B, EDC can be obtained after derivation of the T-matrices.

$$\bar{\varepsilon}=\varepsilon_{1d}+\frac{f(\varepsilon_{1m}Y-\varepsilon_{1d})x}{1+f(x-1)}. \quad (12)$$

By utilizing Eq. (12) and incorporating the properties of chalcogenide glass [14,15], silver from [16-19], gold from [15-24], copper from [24], and titanium dioxide from [25], the dielectric constant of the compound consisting of metallic nanoparticles and glass can be determined [26]. Table 1 presents the magnitude of the EDC $\left(\left|\bar{\varepsilon}\right|\right)$ for chalcogenide glass and metallic nanoparticles and titanium dioxide with 0.08 volume fraction at 635 nm wavelength for three sample radii (obtained using Eq. (12)).

As can be seen in Table 1, at a wavelength of 635 nm and a volume fraction of 0.08, the magnitude of the EDC is strongly dependent on the radius and type of nanoparticles. At 10 nm radius, the smallest EDC is obtained with silver nanoparticles, whereas the largest EDC is obtained with gold nanoparticles. In contrast, at 50 nm radius, the smallest EDC is obtained with gold nanoparticles, whereas the largest EDC is obtained with silver nanoparticles. Finally, at a radius of 100 nm, the smallest EDC is obtained from silver nanoparticles, whereas the largest EDC is obtained from titanium dioxide nanoparticles.

It can be seen in Table 2 that at 635 nm wavelength, the real part of the EDC of chalcogenide glass, when combined with 0.08 volume fraction nanoparticles, is strongly dependent on the type and radius of nanoparticles, such that at 10 nm radius, copper and silver nanoparticles respectively yield the greatest and smallest real part of the EDC. On the other hand, at 50 nm radius, the relationship is reversed, that is, copper and silver nanoparticles respectively yield the smallest and greatest real part of the EDC. Finally, at 100 nm radius, titanium dioxide and silver yield the greatest and smallest real part of the EDC when combined with CG (which is a measure for comparing dispersion).

Similarly, Table 3 presents the imaginary part of the EDC for CG and metallic nanoparticles and Titanium dioxide with 0.08 volume fraction at 635 nm wavelength for 10, 50, and 100 nm radii (which implies the amount of dissipation).

It can be seen in Table 3 that at 635 nm wavelength, the imaginary part of the EDC of chalcogenide glass, when combined with 0.08 volume fraction nanoparticles, is strongly dependent on the type and radius of nanoparticles, such that at all three radii, 10, 50, 100 nm, titanium dioxide nanoparticles yield the smallest imaginary part of the EDC. On the other hand, the situation is different for the greatest imaginary part of the EDC, such that at 10 nm radius gold nanoparticles, at 50 nm copper nanoparticles, and 100 nm radius silver nanoparticles yield the maximum imaginary part.

According to Table 3, the minimum loss in all three sample radii belongs to titanium dioxide, but the maximum loss in different radii is associated with different materials.

In a dielectric function [27-29], the real part underscores the material's ability to store electrical energy (electronic polarizability) and its refractive index, while the imaginary part incorporates the material's energy loss or light absorption.

The dielectric constant is associated with specific materials, such as those used in cable insulation, capacitors, and printed circuit board substrates. It is a complex number with the imaginary part associated with dielectric losses and the real part an indication of the degree to which a material can be polarized [27-29].

Figure 1 shows the EDC of the compound medium versus the nanoparticles radius (a) for five sample volume fractions (f) for silver nanoparticles in CG at 635 nm wavelength, where $\left|\bar{\varepsilon}\right|$, Real $\bar{\varepsilon}$, and Imag $\bar{\varepsilon}$ are the magnitude, real part, and imaginary part of the compound's EDC, respectively.

As can be seen in Fig. 1, the EDC of the compound medium reaches its maximum at 71 nm radius by increasing the nanoparticles volume fraction to 0.1.

Figure 2 shows the magnitude, real part, and imaginary part of the EDC of the compound of CG and copper nanoparticles versus their radius for five volume fractions at 635 nm wavelength.

As shown in Figure 2, the EDC of the compound medium reaches its maximum at 47 nm radius by increasing the nanoparticles volume fraction to 0.1.

In Figure 3, the magnitude, real part, and imaginary part of the EDC of the compound of CG (As_2Se_3) and gold nanoparticles versus their radius (a) at the 635 nm

Table 1. Comparison of magnitude of the EDC for chalcogenide glass, metallic nanoparticles, and Titanium dioxide with 0.08 volume fraction at 635 nm wavelength for three sample radii

Compound	$\left\|\bar{\varepsilon}\right\|$ $a=100nm$	$\left\|\bar{\varepsilon}\right\|$ $a=50nm$	$\left\|\bar{\varepsilon}\right\|$ $a=10nm$
$As_2Se_3-TiO_2$	10.160	9.133	9.026
As_2Se_3-Ag	5.045	10.980	7.751
As_2Se_3-Au	6.266	6.376	10.940
As_2Se_3-Cu	6.101	8.432	10.770

Table 2. The real part of the EDC $\left(\bar{\varepsilon}_{Real}\right)$ for chalcogenide glass and metallic nanoparticles (As_2Se_3) and Titanium dioxide with 0.08 volume fraction at 635 nm wavelength for 10, 50, and 100 nm radii (which implies dispersion).

Compound	$\bar{\varepsilon}_{Real}$ $a=100nm$	$\bar{\varepsilon}_{Real}$ $a=50nm$	$\bar{\varepsilon}_{Real}$ $a=10nm$
$As_2Se_3-TiO_2$	10.150	9.120	9.014
As_2Se_3-Ag	4.889	10.600	7.616
As_2Se_3-Au	6.219	3.783	10.170
As_2Se_3-Cu	6.058	3.423	10.401

Table 3. Comparison of the imaginary part of the EDC for CG As_2Se_3, metallic nanoparticles, and Titanium dioxide with 0.08 volume fraction at 635 nm wavelength for three sample radii.

Compound	$\bar{\varepsilon}_{Imag}$ $a=100nm$	$\bar{\varepsilon}_{Imag}$ $a=50nm$	$\bar{\varepsilon}_{Imag}$ $a=10nm$
As_2Se_3-Ag	1.2450	2.8720	1.4370
As_2Se_3-Au	0.7624	5.1320	4.0330
As_2Se_3-Cu	0.7624	7.7060	2.8130
$As_2Se_3-TiO_2$	0.4968	0.4736	0.4726

wavelength for five sample volume fractions (f) is plotted.

In Figure 3, it can be seen that as the radius of gold nanoparticles approaches 39 nm, EDC reaches its maximum.

Figure 4 shows the magnitude, real part, and imaginary part of the EDC of the compound of CG and titanium dioxide nanoparticles versus their radius for five sample volume fraction.

In Figure 4, it can be seen that by increasing the radius of titanium dioxide nanoparticles and their volume fraction, the EDC increases steeply but, considering plots 1 to 4 and Tables 1 to 3, in the interval 1 to 100 nm the

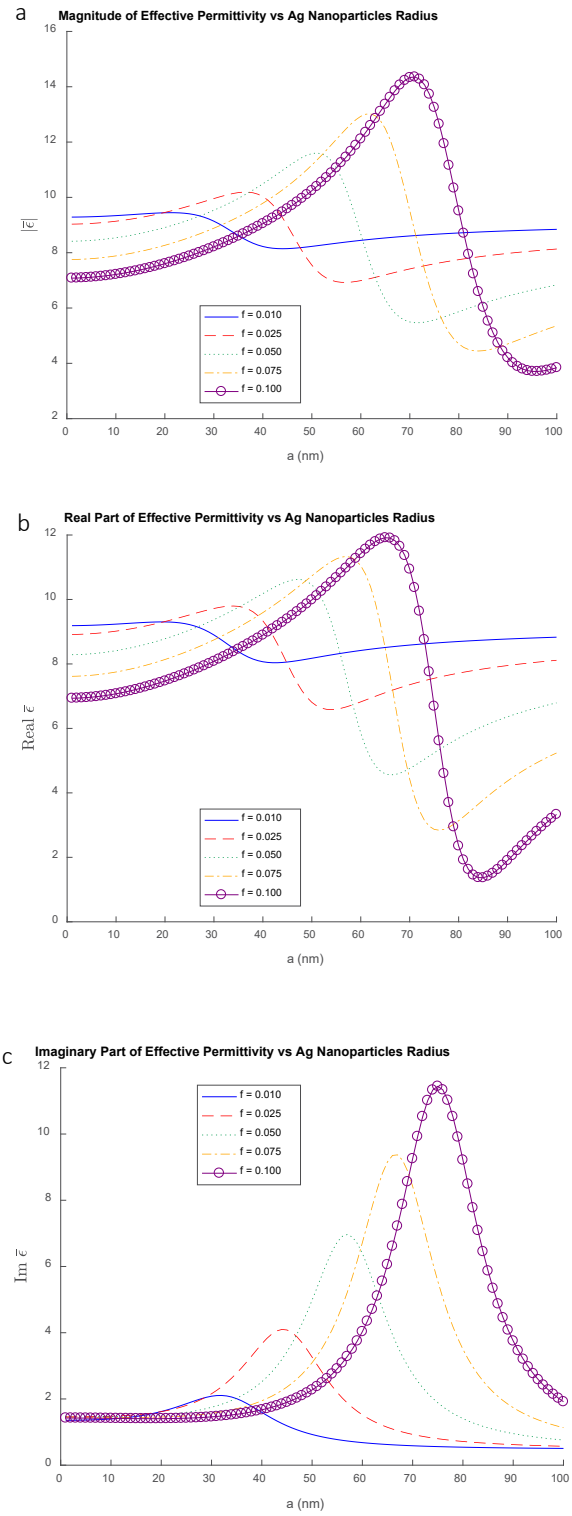

Figure 1. EDC of the compound medium ($\bar{\varepsilon}$) versus the nanoparticles radius (a) at five different volume fractions (f) for silver nanoparticles in CG at 635 nanometer wavelength, where, $|\bar{\varepsilon}|$, Real($\bar{\varepsilon}$) and Imag($\bar{\varepsilon}$) (in parts a, b, c) are the magnitude, real part, and imaginary part of the compound's EDC, respectively.

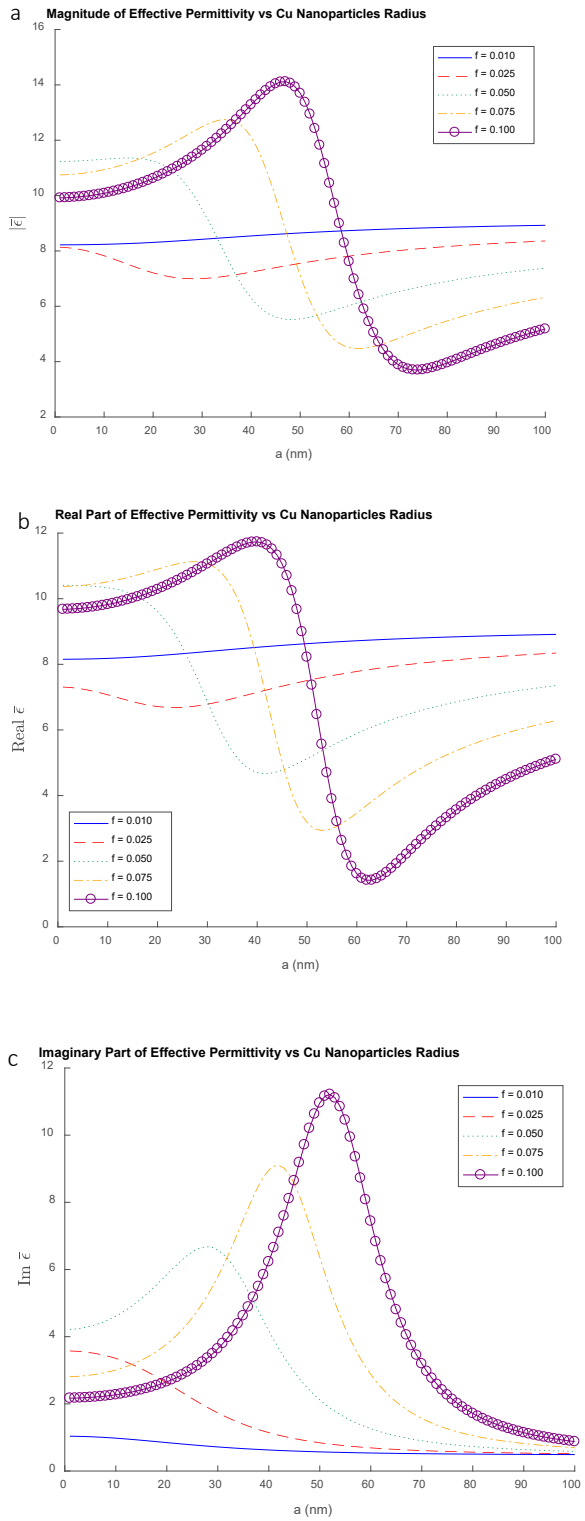

Figure 2. EDC of the compound medium ($\bar{\varepsilon}$) versus the radius (a) at five different volume fractions for copper nanoparticles in CG at 635 nanometer wavelength, where $|\bar{\varepsilon}|$, Real($\bar{\varepsilon}$), Imag($\bar{\varepsilon}$) (in parts a, b, c) are the magnitude, real part, and imaginary part of the compound's EDC, respectively

EDC of CG cannot be increased using titanium dioxide nanoparticles, as well as it can using metallic nanoparticles (silver, copper, and gold). On the other hand, the maximum value of the EDC for these compounds decreases with silver, copper, gold, and titanium dioxide nanoparticles, similarly for the minimum values in an increasing manner.

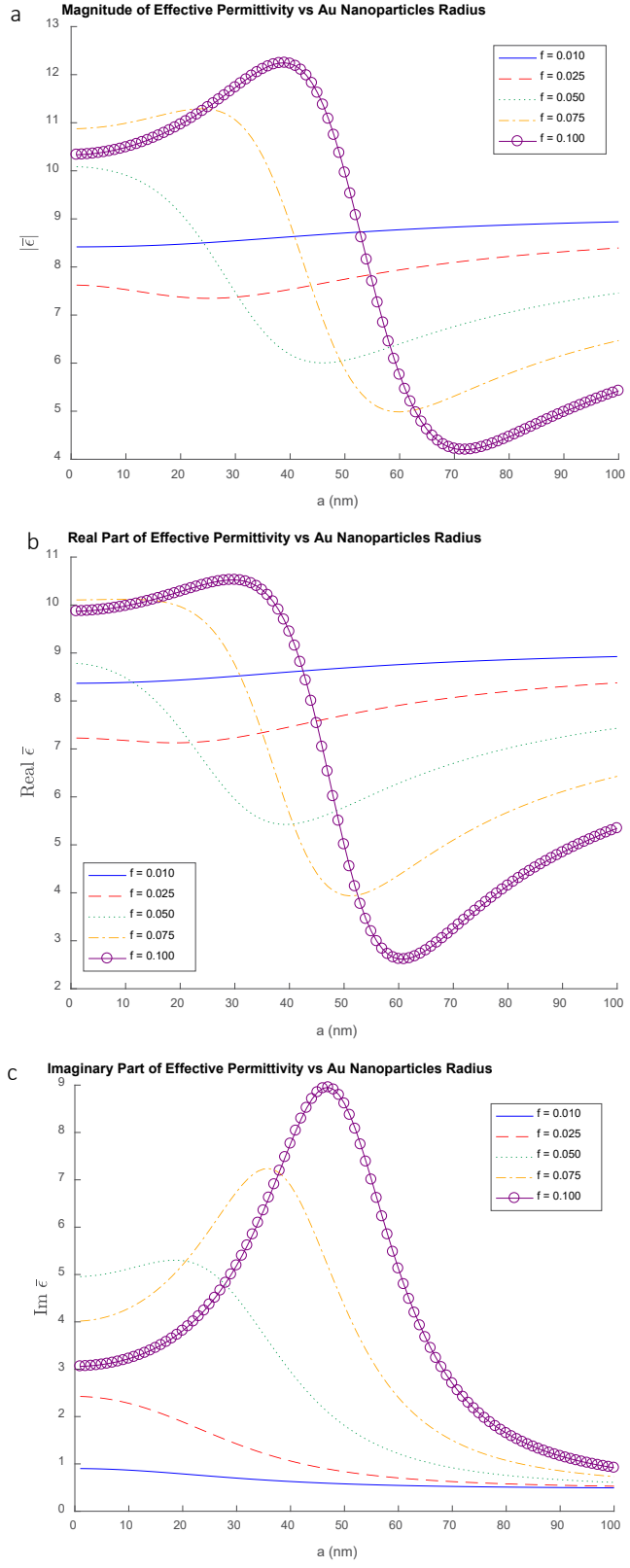

Figure 3. EDC of the compound medium ($\bar{\varepsilon}$) versus the nanoparticles volume radius (a) at five sample fractions (f) for gold nanoparticles in CG at 635 nanometer wavelength, where, $|\bar{\varepsilon}|$, Real ($\bar{\varepsilon}$), Imag($\bar{\varepsilon}$) are the magnitude, real part, and imaginary part of the compound's EDC $\bar{\varepsilon}$, respectively.

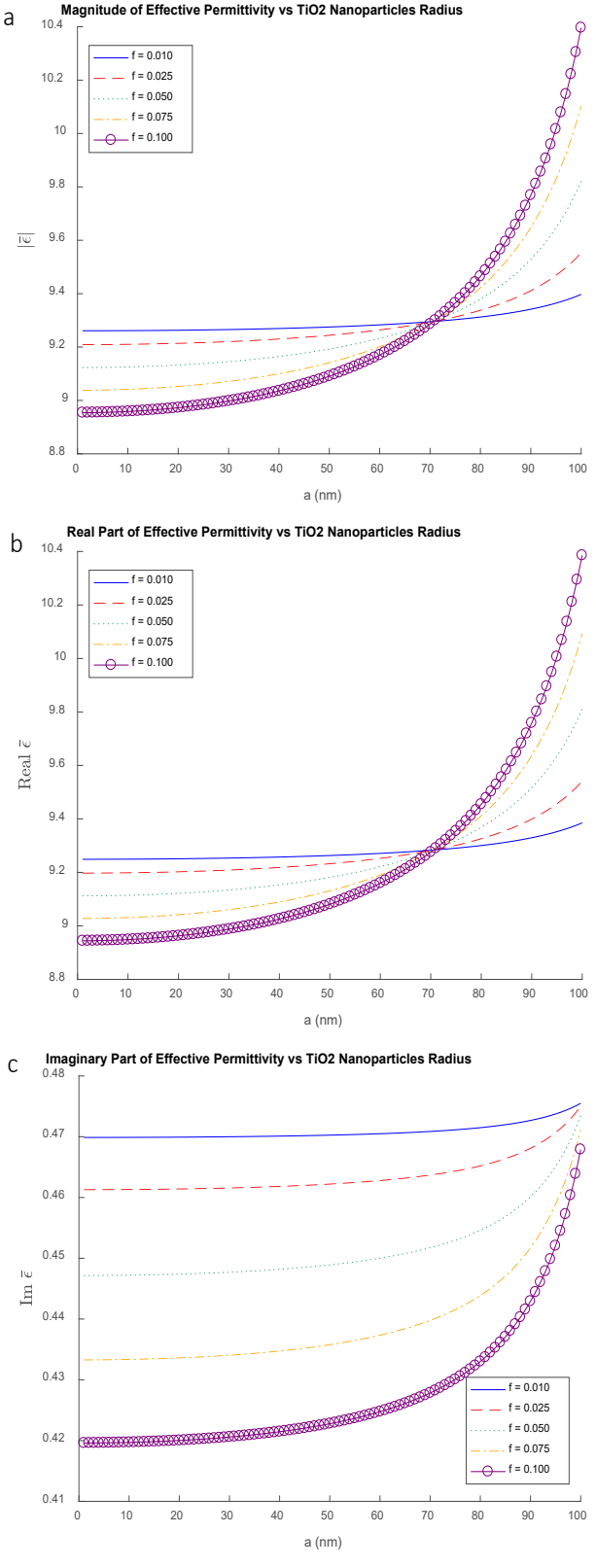

Figure 4. EDC of the compound medium ($\bar{\varepsilon}$) versus their radius (a) for titanium dioxide nanoparticles in CG for five sample volume fractions (f) at 635 nanometer wavelength, where, $|\bar{\varepsilon}|$, Real ($\bar{\varepsilon}$), Imag ($\bar{\varepsilon}$) are the magnitude, real part, and imaginary part of the compound's EDC, respectively

3. Discussion

Even at low volume fractions, specific nanoparticle sizes can resonate with the electromagnetic field, leading to enhanced or diminished EDC due to localized surface plasmon effects [30]. This indicates significant interaction between the nanoparticles and the incident electromagnetic waves, despite the low concentration [30]. The observed maxima and minima likely arise from constructive and destructive interference of light scattered by the nanoparticles [31]. At specific sizes, the scattering cross-section may be optimized, resulting in enhanced EDC (maxima), while at other sizes, destructive interference could lead to reduced EDC (minima). The contrasting dielectric properties of the metal nanoparticles and the host material (chalcogenide or silica glass) can create significant local field enhancements [32-34]. The EDC can peak at nanoparticle sizes where this contrast is most effectively utilized, while at other sizes, it may not contribute positively to the overall dielectric response. At specific radii, the nanoparticles may induce localized electric fields that enhance the local dielectric response. This effect is potentially more pronounced in smaller nanoparticles, where surface effects dominate, possibly leading to maxima in EDC [35]. As the nanoparticle size changes, a transition between different scattering regimes (e.g., Rayleigh scattering for small particles, Mie scattering for intermediate sizes) can occur [36]. This transition can influence how effectively the nanoparticles contribute to the overall permittivity. Nonlinear optical effects might also play a role, even at low concentrations, especially if the electric fields are strong enough to induce polarization changes in the nanoparticles or the surrounding medium [37]. While percolation effects are typically associated with higher volume fractions, critical sizes may exist even at low concentrations where connectivity effects begin to influence the EDC [38]. The T-matrix method was employed to model the EDC of the composite media. Calculations using this model for CG compounds with silver, gold, and copper nanoparticles revealed a significant increase in the EDC with increasing nanoparticle radius, particularly at higher volume fractions. In summary, the presence of maxima and minima in EDC at low nanoparticle volume fractions highlights the complex interactions between the nanoparticles and the host medium. These interactions are influenced by resonance effects, scattering dynamics, and dielectric constant, emphasizing the intricate nature of these composite materials even at low filler concentrations [39]. Further investigation, potentially through numerical modeling or experimental validation, is recommended to gain deeper insights into these phenomena.

4. Conclusion

Consequently, it can be inferred that the material's dielectric losses and dispersion also lack a well-defined monotonic trend, mirroring the fluctuations observed in Figures 1-3. Specifically, the EDC (or its real and imaginary parts) of the medium composed of glasses and silver, copper, and gold nanoparticles does not show a consistent upward or downward trend. The observed fluctuations and the increasing trend in Figure 4 can be explained by several interacting phenomena [1,40-43].
These results are consistent with previous studies [44-46].

5. APPENDICES

5.1. Appendix A: Calculating the Electric Field Vector and the Electric Displacement

The $\bar{\varepsilon}_m$ is the renormalized dielectric constant of metal, which is defined as,

$$\bar{\varepsilon}_m = \varepsilon_m \frac{2F(k_m a)}{1-F(k_m a)}, \quad F(x) = \frac{1}{x^2} - \frac{\cot(x)}{x}, \tag{A.1}$$

Note that using Eq. (A.1), it follows that

$$F(k_m a) = \frac{1}{(k_m a)^2} - \frac{\cot(k_m a)}{k_m a} \tag{A.2}$$

$$\bar{\varepsilon}_m = \varepsilon_{1m} \times \left(2[\frac{1}{(k_m a)^2} - \frac{\cot(k_m a)}{k_m a}] \right) \Big/ \tag{A.3}$$

$$\left(1 - [\frac{1}{(k_m a)^2} - \frac{\cot(k_m a)}{k_m a}] \right) + \varepsilon_{2m} \left| \vec{E} \right|^2$$

Since the first term in Eq. (A.3) (fractional part) is independent of the electric field, using a change of variable, it follows that

$$\bar{\varepsilon}_m = \varepsilon_{1m} Y + \varepsilon_{2m} \left| \vec{E} \right|^2, \tag{A.4}$$

$$Y = \left(2[\frac{1}{(k_m a)^2} - \frac{\cot(k_m a)}{k_m a}] \right) \Big/ \left(1 - [\frac{1}{(k_m a)^2} - \frac{\cot(k_m a)}{k_m a}] \right)$$

Using substitution, we can write

$$\varepsilon_e = \varepsilon_d \frac{(1+2f)[\varepsilon_{1m} Y + \varepsilon_{2m} \left| \vec{E} \right|^2] + 2(1-f)\varepsilon_d}{(1-f)[\varepsilon_{1m} Y + \varepsilon_{2m} \left| \vec{E} \right|^2] + (f+2)\varepsilon_d} \tag{A.5}$$

On the other hand, the host medium also has nonlinear properties, and its dielectric constant is related to the electric field as

$$\varepsilon_d = \varepsilon_{1d} + \varepsilon_{2d} \left| \vec{E}_0 \right|^2 \tag{A.6}$$

$$\varepsilon_e = (\varepsilon_{1d} + \varepsilon_{2d} \left| \vec{E}_0 \right|^2) \tag{A.7}$$

$$\frac{(1+2f)[\varepsilon_{1m} Y + \varepsilon_{2m} \left| \vec{E} \right|^2] + 2(1-f)(\varepsilon_{1d} + \varepsilon_{2d} \left| \vec{E}_0 \right|^2)}{(1-f)[\varepsilon_{1m} Y + \varepsilon_{2m} \left| \vec{E} \right|^2] + (f+2)(\varepsilon_{1d} + \varepsilon_{2d} \left| \vec{E}_0 \right|^2)}$$

The expression for the electric field within the nanoparticles is provided as follows:

$$\vec{E} = \frac{3\varepsilon_e}{2\varepsilon_e + \overline{\varepsilon}_m}\vec{E}_0, \tag{A.8}$$

Substituting Eq. (A.3) and Eq. (A.7) into Eq. (A.8) yields

$$\vec{E} = \frac{3\varepsilon_e}{2\varepsilon_e + \varepsilon_{1m}\dfrac{2F(k_m a)}{1-F(k_m a)} + \varepsilon_{2m}\left|\vec{E}\right|^2}\vec{E}_0 \tag{A.9}$$

$$\begin{aligned}\vec{E} = x\vec{E}_0 &- \frac{x[3\varepsilon_{1d}(1+2f)\varepsilon_{2m}(Y+1)]}{3\varepsilon_{1d}(1+2f)\varepsilon_{1m}Y + 6\varepsilon_{1d}^2(1-f)}\left|\vec{E}\right|^2\vec{E}_0 \\ &- \frac{x[\varepsilon_{1d}(5f+4)\varepsilon_{2m}(Y+1) + (1-f)(2\varepsilon_{1m}Y\varepsilon_{2m})(Y+1)]}{3\varepsilon_{1d}(1+2f)\varepsilon_{1m}Y + 6\varepsilon_{1d}^2(1-f)}\left|\vec{E}\right|^2\vec{E} \\ &- \frac{x(1-f)\varepsilon_{2m}^2(Y+1)^2}{3\varepsilon_{1d}(1+2f)\varepsilon_{1m}Y + 6\varepsilon_{1d}^2(1-f)}\left|\vec{E}\right|^4\vec{E}.\end{aligned} \tag{A.10}$$

$$x = \frac{3\varepsilon_{1d}(1+2f)\varepsilon_{1m}Y + 6\varepsilon_{1d}^2(1-f)}{\varepsilon_{1d}(5f+4)\varepsilon_{1m}Y + (1-f)(4\varepsilon_{1d}^2 + \varepsilon_{1m}^2Y^2)} \tag{A.11}$$

Now, by evaluating $\left|\vec{E}\right|^2 (= \vec{E}\cdot\vec{E}^*)$ and $\left|\vec{E}\right|^4$, and ignoring terms with order greater than 5, we can write

$$\vec{E} = x\vec{E}_0 - x\alpha\left|\vec{E}\right|^2\vec{E}_0 - x\beta\left|\vec{E}\right|^2\vec{E} - x\gamma\left|\vec{E}\right|^4\vec{E}, \tag{A.12}$$

where $\alpha, \beta \text{ and } \gamma$ are defined as,

$$\begin{aligned}\alpha &= \frac{3\varepsilon_{1d}(1+2f)\varepsilon_{2m}(Y+1)}{3\varepsilon_{1d}(1+2f)\varepsilon_{1m}Y + 6\varepsilon_{1d}^2(1-f)}, \\ \beta &= \frac{\varepsilon_{1d}(5f+4)\varepsilon_{2m}(Y+1) + (1-f)(2\varepsilon_{1m}Y\varepsilon_{2m})(Y+1)}{3\varepsilon_{1d}(1+2f)\varepsilon_{1m}Y + 6\varepsilon_{1d}^2(1-f)}, \\ \gamma &= \frac{(1-f)\varepsilon_{2m}^2(Y+1)^2}{3\varepsilon_{1d}(1+2f)\varepsilon_{1m}Y + 6\varepsilon_{1d}^2(1-f)}.\end{aligned} \tag{A.13}$$

$$\begin{aligned}\vec{E} = x\vec{E}_0 &+ x(\alpha\vec{E}_0 - \beta\vec{E})[|x|^2\left|\vec{E}_0\right|^2\left|\vec{E}\right|^2 + \alpha^*|x|^2\left|\vec{E}_0\right|^2\left|\vec{E}\right|^2 \\ &- \beta^*|x|^2\left|\vec{E}\right|^2(\vec{E}_0\cdot\vec{E}^*) + \alpha|x|^2\left|\vec{E}_0\right|^2\left|\vec{E}\right|^2 \\ &- \beta|x|^2\left|\vec{E}\right|^2(\vec{E}\cdot\vec{E}_0{}^*)] - x\gamma|x|^4\left|\vec{E}_0\right|^4\vec{E}.\end{aligned} \tag{A.14}$$

Using Eq. (A-12), if $\vec{E}$ is approximately replaced by $x\vec{E}_0$ in Eq. (A-14), it follows that

$$\begin{aligned}\vec{E} &= x\vec{E}_0 + x(\alpha-\beta x)|x|^2\left|\vec{E}_0\right|^2\vec{E}_0 \\ &+[x(\alpha-\beta x)(\alpha^* - \beta^*x^* + \alpha - \beta x) - \\ &x^2\gamma]|x|^4\left|\vec{E}_0\right|^4\vec{E}_0,\end{aligned} \tag{A.15}$$

and the electric displacement vector is given by

$$\vec{D} = \overline{\varepsilon}_m\vec{E}. \tag{A.16}$$

5.2. Appendix B: Derivation of the T-matrices and Obtaining EDC

Using the average Eq. (10) and equating it with the same order terms in Eq. (A.15), it follows that

$$\begin{aligned}&1 + \langle GT^{(1)}\rangle = x, \quad 4\pi\langle GT^{(3)}\rangle = x(\alpha-\beta x)|x|^2, \\ &4\pi\langle GT^{(5)}\rangle = x[(\alpha-\beta x)(\alpha^* - \beta^*x^* + \alpha - \beta x) - x\gamma]|x|^4\end{aligned} \tag{B.1}$$

Furthermore, using the average $\vec{D}$ (Eq. (11)) and equating it with the same order terms in Eq. (A.16), it follows that

$$\begin{aligned}&\varepsilon_{1d}(1+\langle GT^{(1)}\rangle) + \langle T^{(1)}\rangle \\ &= \varepsilon_{1m}Yx4\pi(\varepsilon_{1d}\langle GT^{(3)}\rangle + \langle T^{(3)}\rangle) \\ &= [\varepsilon_{1m}(\alpha-\beta x)Y + \varepsilon_{2m}(Y+1)]x|x|^2\,4\pi(\varepsilon_{1d}\langle GT^{(5)}\rangle + \langle T^{(5)}\rangle) \\ &= \{\varepsilon_{1m}Y[x(\alpha-\beta x)(\alpha^* - \beta^*x^* + \alpha - \beta x) - x^2\gamma] \\ &+\varepsilon_{2m}(Y+1)x(\alpha-\beta x)\}|x|^4\end{aligned} \tag{B.2}$$

Next, Eq (B-1) can be expressed as

$$\begin{aligned}&\langle GT^{(1)}\rangle = x-1, \\ &\langle GT^{(3)}\rangle = \frac{1}{4\pi}x(\alpha-\beta x)|x|^2, \\ &\langle GT^{(5)}\rangle = \frac{1}{4\pi}x[(\alpha-\beta x)(\alpha^* - \beta^*x^* + \alpha - \beta x) - x\gamma]|x|^4\end{aligned} \tag{B.3}$$

and it follows from Eq. (B.1) and Eq. (B.3) that

$$\begin{aligned}&\langle T^{(1)}\rangle = (\varepsilon_{1m}Y - \varepsilon_{1d})x, \\ &\langle T^{(3)}\rangle = \frac{x}{4\pi}|x|^2[(\alpha-\beta x)(\varepsilon_{1m}Y - \varepsilon_{1d}) + \varepsilon_{2m}(Y+1)], \\ &\langle T^{(5}\rangle = \frac{x}{4\pi}|x|^4\{(\varepsilon_{1m}Y - \varepsilon_{1d})\times[(\alpha-\beta x)| \\ &(\alpha^* - \beta^*x^* + \alpha - \beta x) - x\gamma] + \varepsilon_{2m}(Y+1)(\alpha-\beta x)\}\end{aligned} \tag{B.4}$$

In the compound medium, the outcomes can be generalized by removing factors such as overlapping. This implies that the T-matrix of the compound medium is assumed to be the sum of the T-matrices of each guest particle. Considering the volume fraction of the nanoparticles f, Eq. (B.3) can be expressed in a revised form.

$$\langle GT^{(1)}\rangle = f(x-1), \tag{B.5-a}$$

$$\langle GT^{(3)}\rangle = \frac{f}{4\pi}x(\alpha-\beta x)|x|^2, \tag{B.5-a}$$

$$\langle GT^{(5)}\rangle = \frac{f}{4\pi}x[(\alpha-\beta x)(\alpha^* - \beta^*x^* + \alpha - \beta x) - x\gamma]|x|^4 \tag{B.5-a}$$

Similarly, Eq. (B.4) can be expressed as

$$\langle T^{(1)}\rangle = f(\varepsilon_{1m}Y - \varepsilon_{1d})x \tag{B.6-a}$$

$$\langle T^{(3)}\rangle = \frac{f}{4\pi}x|x|^2[(\alpha-\beta x)(\varepsilon_{1m}Y - \varepsilon_{1d}) + \varepsilon_{2m}(Y+1)] \tag{B.6-a}$$

$$\begin{aligned}\langle T^{(5}\rangle = \frac{f}{4\pi}x|x|^4\{(\varepsilon_{1m}Y - \varepsilon_{1d})[(\alpha-\beta x) \\ (\alpha^* - \beta^*x^* + \alpha - \beta x) - x\gamma] + \varepsilon_{2m}(Y+1)(\alpha-\beta x)\}\end{aligned} \tag{B.6-a}$$

Using the T-matrix method, the EDC can be obtained as

$$\bar{\varepsilon} = \varepsilon_{1d} + \frac{\langle T^{(1)} \rangle}{1 + \langle G T^{(1)} \rangle} \quad \text{(B.7)}$$

By substituting Eq. (B.5.a) and Eq. (B.6.a) into Eq. (B.7), it follows that

$$\bar{\varepsilon} = \varepsilon_{1d} + \frac{f(\varepsilon_{1m} Y - \varepsilon_{1d})x}{1 + f(x-1)} \quad \text{(B.8)}$$

CONFLICT OF INTEREST

The authors declare that they have no conflict of interest.

DATA AVAILABILITY STATEMENT

This manuscript has associated data in a data repository. Data will be made available on request.

REFERENCES

1. Zakery A, Elliott SR. Optical properties and applications of chalcogenide glasses: a review. J Non-Cryst Solids. 2003;330:1-12. https://doi.org/10.1016/j.jnoncrysol.2003.08.064
2. Ogusu K, Yamasaki J, Maeda S, Kitao M, Minikata M. Linear and nonlinear optical properties of Ag-As-Se chalcogenide glass for all-optical switching. Opt Lett. 2004;29(3):265-267. https://doi.org/10.1364/OL.29.000265
3. Brandes RG, Laming FP, Pearson AD. Optically formed dielectric gratings in thick films of arsenic-sulfur glass. Appl Opt. 1970;9(7):1712-1714. https://doi.org/10.1364/AO.9.001712
4. Garnett JM. Colours in metal glasses, in metallic films, and in metallic solutions. II. Philos Trans R Soc Lond A. 1906;205(387-401):237-288. https://doi.org/10.1098/rsta.1906.0007
5. Wang G, Zhang Y, Liu J, Chen W, Wang K, Cui B, et al. Dispersion hardening using amorphous nanoparticles deployed via additive manufacturing. Nat Commun. 2025;16(1):3589. https://doi.org/10.1038/s41467-025-58893-1
6. Waterman PC. T-matrix methods in acoustic scattering. J Acoust Soc Am. 2009;125(1):42-51. https://doi.org/10.1121/1.3035839
7. Qi X, Nieminen TA, Stilgoe SB, Loke VLY, Rubinsztein-Dunlop H. Comparison of T-matrix calculation methods for scattering by cylinders in optical tweezers. Opt Lett. 2014;39(16):4827-4830. https://doi.org/10.1364/OL.39.004827
8. Gharaati A, Kamaldar A. Enhancement of nonlinear optical properties of compounds of silica glass and metallic nanoparticle. Pramana. 2016;86:1329-1342. https://doi.org/10.1007/s12043-015-1185-3
9. Sayrac M, Dakhlaoui H, Mora-Ramos ME, Ungan F. Exploring the nonlinear optical behaviour of InGaAs/GaAs triple quantum wells via structural modulations and external electric fields. Int J Nanosci Nanotechnol. 2023;19(4):249-262.
10. Bay MA, Khademieslam H, Bazyar B, Najafi A, Hemmasi AH. Mechanical and thermal properties of nanocomposite films made of polyvinyl alcohol/nanofiber cellulose and nanosilicon dioxide using ultrasonic method. Int J Nanosci Nanotechnol. 2021;17(2):65-76. https://doi.org/10.15376/biores.17.1.1031-1046
11. Nadafan M, Malekfar R, Dehghani Z. Investigation into properties of polyurethane closed cell by high loading of SiO2 nanoparticles. Int J Nanosci Nanotechnol. 2015;11(3):185-192.
12. Brown RG. Classical electrodynamics. Durham (NC): Duke University Physics Department; 2009. Report No.: 27708-0305.
13. Sarychev AK, Shalaev VM. Electromagnetic field fluctuations and optical nonlinearities in metal-dielectric composites. Phys Rep. 2000;335(6):275-371. https://doi.org/10.1016/S0370-1573(99)00118-0
14. Joseph S, Sarkar S, Joseph J. Grating-coupled surface plasmon-polariton sensing at a flat metal-analyte interface in a hybrid-configuration. ACS Appl Mater Interfaces. 2020;12(41):46519-46529. https://doi.org/10.1021/acsami.0c12525
15. Joseph S, Sarkar S, Khan S, Joseph J. Exploring the optical bound state in the continuum in a dielectric grating coupled plasmonic hybrid system. Adv Opt Mater. 2021;9(8):2001895. https://doi.org/10.1002/adom.202001895
16. Ciesielski A, Skowronski L, Trzcinski M, Szoplik T. Controlling the optical parameters of self-assembled silver films with wetting layers and annealing. Appl Surf Sci. 2017;421:349-356. https://doi.org/10.1016/j.apsusc.2017.01.039
17. Choi J, Cheng F, Cleary JW, Sun L, Dass CK, Hendrickson JR, et al. Optical dielectric constants of single crystalline silver films in the long wavelength range. Opt Mater Express. 2020;10(2):693-703. https://doi.org/10.1364/OME.385723
18. Jiang Y, Pillai S, Green MA. Realistic silver optical constants for plasmonics. Sci Rep. 2016;6:30605. https://doi.org/10.1038/srep30605
19. McPeak KM, Jayanti SV, Kress SJ, Meyer S, Iotti S, Rossinelli A, et al. Plasmonic films can easily be better: rules and recipes. ACS Photonics. 2015;2(3):326-333. https://doi.org/10.1021/ph5004237
20. Rosenblatt G, Simkhovich B, Bartal G, Orenstein M. Nonmodal plasmonics: controlling the forced optical response of nanostructures. Phys Rev X. 2020;10(1):011071. https://doi.org/10.1103/PhysRevX.10.011071
21. Yakubovsky DI, Arsenin AV, Stebunov YV, Fedyanin DY, Volkov VS. Optical constants and structural properties of thin gold films. Opt Express. 2017;25(21):25574-25587. https://doi.org/10.1364/OE.25.025574
22. Yakubovsky DI, Stebunov YV, Kirtaev RV, Ermolaev GA, Mironov MS, Novikov SM, et al. Ultrathin and ultrasmooth gold films on monolayer MoS2. Adv Mater Interfaces. 2019;6(13):1900196. https://doi.org/10.1002/admi.201900196
23. Ciesielski A, Skowronski L, Trzcinski M, Górecka E, Trautman P, Szoplik T. Evidence of germanium segregation in gold thin films. Surf Sci. 2018;674:73-78. https://doi.org/10.1016/j.susc.2018.03.020
24. Babar S, Weaver JH. Optical constants of Cu, Ag, and Au revisited. Appl Opt. 2015;54(3):477-481. https://doi.org/10.1364/AO.54.000477
25. Bodurov I, Vlaeva I, Viraneva A, Yovcheva T, Sainov S. Modified design of a laser refractometer. Nanosci Nanotechnol. 2016;16:31-33.
26. Shahmirzaee H, Gharaati A, Kamaldar A. Investigating the effect of the size of metal nanoparticles on increasing the optical properties of glasses using the T-matrix method. Optoelectron Adv Mater. 2022;4:105-113.
27. Wang H, Yang L. Dielectric constant, dielectric loss, conductivity, capacitance and model analysis of electronic electroactive polymers. Polym Test. 2023;120:107965. https://doi.org/10.1016/j.polymertesting.2023.107965
28. Nidhi, Modgil V, Rangra VS. Dielectric dispersion in Te9Se72Ge19-xSbx (x = 8, 9, 10, 11, 12) chalcogenide glassy alloy. Chalcogenide Lett. 2016;13(8):359-371.
29. Guo S, Wu F, Albin S, Tai H, Rogowski RS. Loss and dispersion analysis of microstructured fibers by finite-difference method. Opt Express. 2004;12(15):3341-3352. https://doi.org/10.1364/OPEX.12.003341
30. Kelly KL, Coronado E, Zhao LL, Schatz GC. The optical properties of metal nanoparticles: the influence of size, shape, and dielectric environment. J Phys Chem B. 2003;107(3):668-677. https://doi.org/10.1021/jp026731y
31. Guzman-Sepulveda JR, Dogariu A. Multimode interference dynamic light scattering. Opt Lett. 2018;43(17):4232-4235. https://doi.org/10.1364/OL.43.004232
32. Cai Z, Wang X, Luo B, Hong W, Wu L, Li L. Nanocomposites with enhanced dielectric permittivity and breakdown strength by microstructure design of nanofillers. Compos

Sci Technol. 2017;151:109-114. https://doi.org/10.1016/j.compscitech.2017.08.015
33. Decrossas E, El Sabbagh MA, Naseem HA, Hanna VF, El-Ghazaly SM. Effective permittivity extraction of dielectric nano-powder and nano-composite materials: effects of packing densities and mixture compositions. In: 2011 41st European Microwave Conference (EuMC). IEEE; 2011. p. 956-959. https://doi.org/10.23919/EuMC.2011.6101818
34. Hou Y, Wang G, Ma C, Feng Z, Chen Y, Filleter T. Quantification of the dielectric constant of MoS2 and WSe2 nanosheets by electrostatic force microscopy. Mater Charact. 2022;193:112313. https://doi.org/10.1016/j.matchar.2022.112313
35. Schmid M, Andrae P, Manley P. Plasmonic and photonic scattering and near fields of nanoparticles. Nanoscale Res Lett. 2014;9:1-11. https://doi.org/10.1186/1556-276X-9-50
36. Wang X, Cao Y. Characterizations of absorption, scattering, and transmission of typical nanoparticles and their suspensions. J Ind Eng Chem. 2020;82:324-332. https://doi.org/10.1016/j.jiec.2019.10.030
37. Rao AS. Saturation effects in nonlinear absorption, refraction, and frequency conversion: a review. Optik. 2022;267:169638. https://doi.org/10.1016/j.ijleo.2022.169638
38. Fralick BS, Gatzke EP, Baxter SC. Three-dimensional evolution of mechanical percolation in nanocomposites with random microstructures. Probabilist Eng Mech. 2012;30:1-8. https://doi.org/10.1016/j.probengmech.2012.02.002
39. Jebbor N, Bri S. Effective permittivity of periodic composite materials: numerical modeling by the finite element method. J Electrost. 2012;70(4):393-399. https://doi.org/10.1016/j.elstat.2012.05.007
40. Heiba ZK, Abozied AM, Ahmed SI, Abdellatief M, Mohamed MB. Effect of metal chalcogenides on modifying the structural and optical properties of ZnWO4 nanostructure. Opt Mater. 2024;158:115717. https://doi.org/10.1016/j.optmat.2024.115717
41. Singla S, Lal B, Kaur J, Sharma G. Optical behavior of glasses containing gold nanoparticles: a review. Opt Laser Technol. 2024;174:110675. https://doi.org/10.1016/j.optlastec.2024.110675
42. Iyer NV, Agawane GL, Patel C, Kher JA, Bhame SD. Contemporary advances in metal oxide doped polypyrrole composites: a comprehensive review. Int J Nanosci Nanotechnol. 2024;20(2):143-159. https://doi.org/10.22034/ijnn.2024.2005501.2391
43. Ma R, Cui B, Hu D, Wang Y, Zhao W, Tian M. Improving the dielectric properties of the Ba(Zr0.1Ti0.9)O3-based ceramics by adding a Li2O-SiO2 sintering agent step by step. Int J Nanosci Nanotechnol. 2020;16(4):233-241.
44. Trakhtenberg LI, Kozhushner MA, Gerasimov GN, Gromov VF, Bodneva VL, Antropova TV, et al. Non-phenomenological description of complex dielectric permittivity of metal-containing porous glasses. J Non-Cryst Solids. 2010;356(11-17):642-646. https://doi.org/10.1016/j.jnoncrysol.2009.06.051
45. Sachin, Pandey BK, Jaiswal RL. Modelling the dielectric constant and refractive index of semiconducting nanoparticles. J Opt. 2025;54(1):61-70. https://doi.org/10.1007/s12596-025-02453-9
46. Gerace KS, Lanagan MT, Mauro JC. Dielectric polarizability of SiO2 in niobiosilicate glasses. J Am Ceram Soc. 2023;106(8):4546-4553. https://doi.org/10.1111/jace.19151